A VISIBLE-LIGHT MONITOR FOR TRANSVERSE BEAM PROFILE DIAGNOSTICS IN THE SLS BOOSTER

M. P. Rey Barrera*, J. Kallestrup, R. Ischebeck, M. Seidel, L. Zimmermann
PSI Center for Accelerator Science and Engineering, Villigen, Switzerland

Abstract

A visible-light 2D imaging monitor was developed and commissioned in the Swiss Light Source (SLS) 2.0 booster ring to characterize transverse beam behavior during the energy ramp. Installed downstream of a bending magnet, it extracts visible synchrotron radiation via an in-vacuum gold-coated mirror and uses a CMOS camera with motorized optics and filters. The setup accommodates the evolving synchrotron spectrum, with the critical photon energy increasing from 0.2 eV at 100 MeV electron beam energy to approximately 3.9 keV at 2.7 GeV. Long exposures, integrating over hundreds of turns matched to the roughly 1 µs revolution time, enabled measurements of adiabatic damping due to synchrotron radiation emission. In addition, the system provides sufficient sensitivity to image single-bunch charges down to approximately 20 pC, while operating over a broad charge range up to 300 pC. Using short exposures over only a few tens of turns enabled the observation of fast beam size evolution during emittance exchange driven by coupling resonance crossing, a technique first implemented in an electron ring at the SLS. This high-speed acquisition confirmed the optimal extraction timing, corresponding to the minimum horizontal beam size. The monitor provides non-invasive diagnostics for tracking beam stability and optimizing injection into the storage ring.

INTRODUCTION

Injection into fourth-generation synchrotron light sources is challenging due to the reduced dynamic aperture of the storage ring. To ensure efficient injection, the injector must deliver a beam with well-controlled transverse properties and sufficiently small emittance. For SLS 2.0, the injector is a low-emittance booster synchrotron [1], which accelerates the beam to the nominal storage-ring injection energy of 2.7 GeV. In addition, transverse emittance exchange during coupling resonance crossing is implemented near the end of the booster ramp to further reduce the horizontal beam size before extraction [2, 3].

Knowledge of the transverse beam properties throughout the ramp is therefore essential to verify the beam quality delivered by the booster. This is particularly important during the short emittance-exchange process, where the transverse beam sizes evolve rapidly over only a few milliseconds. A non-invasive diagnostic capable of resolving the beam profile at different times during the ramp is therefore required both for commissioning and for routine optimization of the injected beam.

* maria.rey-barrera@psi.ch

The most practical, non-destructive method to measure emittance is through synchrotron radiation (SR). From measurements of the beam profile, parameters like emittance and energy spread can be inferred. In order to measure the beam size evolution during the ramp and the emittance exchange process, we generally require fast acquisition, variable trigger timing, and the ability to handle large intensity variations. Synchrotron light from the booster has previously been used for beam diagnostics at other facilities, such as for transverse beam shape at the ESRF [4], bunch duration monitors at the APS [5], SOLEIL [6], and ELSA [7].

Table 1: Twiss parameters at the extraction point of the bend magnet.

Parameter	Value
β_x [m]	1.9950
β_y [m]	11.1432
α_x	−0.3494
α_y	−0.2005
η_x [m]	0.1864
η'_x	0.0044

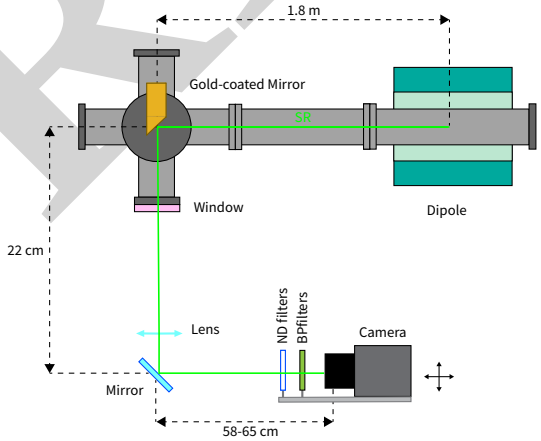

Figure 1: Schematic of the optical system, showing the SR propagating from the in-vacuum gold-coated mirror, to the lens, bandpass (BP) and ND filters, and camera.

EXPERIMENTAL SETUP

The diagnostic system is installed inside the booster tunnel, downstream of a 1.26 m dipole magnet with bend radius of 11.21 m, operating from 0.03 to 0.803 T at 100 MeV and 2.7 GeV electron beam energies respectively during ramp up. It is located 19.5 m before the entrance of the injection septum. The source point is located at the middle of the dipole magnet, where the Twiss parameters are those found in Table 1, and the vertical dispersion is negligible.

The diagnostic station extracts visible SR from the booster vacuum chamber, which has an elliptical inner aperture of approximately 30 mm × 20 mm. The radiation is first intercepted by an in-vacuum plane deflection mirror with a 35 mm aperture and a 96° mechanical angle. This mirror is made of OFHC copper and plasma coated with gold. As shown in Fig. 1, downstream of the vacuum chamber, the light passes through a sapphire window and is remotely steered by a motorized mirror. The light then passes through remotely controlled bandpass and neutral density (ND) filters before being focused by a plano-convex lens onto a CMOS camera.

To minimize chromatic aberrations in the imaging system, the presented results were obtained using 442 and 532 nm bandpass filters, which also provided sufficient intensity for reliable beam size measurements throughout the ramp. A fixed source-lens distance of ~ 1.8 m and a lens focal length of 493.57 and 499.31 mm resulted in demagnification factors of 0.38 and 0.39 for the chosen wavelengths, 442 and 532 nm, respectively.

Error Sources

Because SR is emitted over an extended and curved trajectory in the bending magnet, depth of field contributes in both transverse planes, while source curvature contributes only in the horizontal plane. Following Clarke [8], the effective source length and depth of field blur are estimated as $L_{\mathrm{eff}} \simeq 2R(\theta_{\mathrm{acc}} + \psi_{\mathrm{SR}})$ and $r_f \simeq L_{\mathrm{eff}}\theta_{\mathrm{acc}}/2$, where R is the bending radius, θ_{acc} is the optical half acceptance angle, and ψ_{SR} is the natural SR opening angle. The half acceptance angle was calculated using the Hofmann–Méot formalism [9].

For the SLS booster bend radius, the natural visible-light opening angles are $\psi_{\mathrm{SR}} = 2.11$ mrad at 442 nm and $\psi_{\mathrm{SR}} = 2.25$ mrad at 532 nm. At injection energy, the calculated half acceptance angles are 1.02 mrad and 1.08 mrad, giving vertical rms depth-of-field contributions of 20.5 µm and 23.2 µm, respectively. In the horizontal plane, the additional curvature term, $r_c \simeq R\theta_{\mathrm{acc}}^2/2$ [8], contributes 3.3 µm and 3.8 µm rms. Combining both terms in quadrature gives total horizontal rms optical contributions of 20.8 µm at 442 nm and 23.5 µm at 532 nm.

Above about 250 MeV, θ_{acc} becomes equal to the natural visible-light opening angle. The vertical rms depth-of-field contributions are then 57.7 µm and 65.3 µm at 442 nm and 532 nm, respectively. The corresponding curvature terms are 14.4 µm and 16.3 µm rms, resulting in total horizontal rms optical contributions of 59.5 µm and 67.3 µm.

Finally, since the lens is operated with a large aperture, the image quality is expected to suffer from significant spherical aberration. This contribution has not yet been experimentally quantified and remains part of the future characterization of the system. Therefore, the beam size values reported in this work are corrected only for the depth of field and curvature contributions discussed above. A dedicated measurement of the spherical-aberration contribution is still required, for example using a Shack-Hartmann wavefront sensor. Once quantified, the corresponding image-plane blur can be included in the total resolution term and subtracted from the measured beam size. The aberration may also be reduced by reversing the orientation of the plano-convex lens, with the convex side facing the incoming light.

BEAM SIZE MEASUREMENTS

To study beam dynamics in the booster, the exposure time was chosen with respect to the roughly 1 µs revolution period, and 19-20 measurements were acquired at different time delays relative to the start of the ramp. The beam size evolution during acceleration, including the effects of adiabatic damping and SR energy loss, was examined using a 300 µs exposure aligned with the 320 ms SLS booster energy ramp. During this ramp, the beam is accelerated from the low injection energy to the nominal extraction energy of 2.7 GeV; extraction occurs at about 160 ms into the ramp, corresponding to a camera delay of approximately 150 ms. The full ramp then continues with a down-ramp before the next beam injection. In this measurement, the beam was intentionally not extracted at the usual extraction time to allow observation over the full ramp.

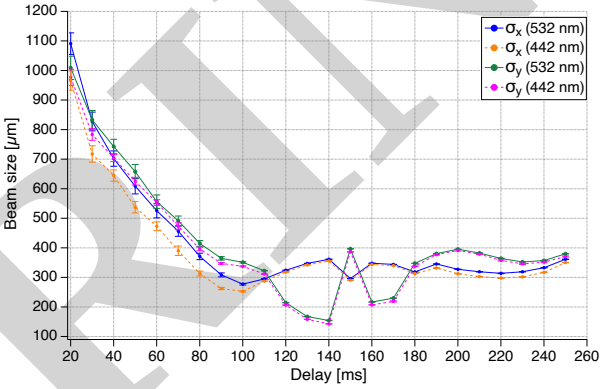

Figure 2: Time evolution of the horizontal (σ_x) and vertical (σ_y) beam sizes during the ramp, measured with a 300 µs exposure time using 442 nm and 532 nm bandpass filters.

Figure 2 shows highly similar beam-size evolution for both wavelengths throughout the ramp. Between 20 and 140 ms, σ_x decreases by about 63–67%, while σ_y decreases by about 85% for both 442 and 532 nm. The 532 nm measurements are systematically larger than the 442 nm measurements by approximately 7% in σ_x and 4% in σ_y over the full ramp. The standard deviations are largest at the beginning of the ramp, where the beam is larger and less stable, and decrease substantially toward 140 ms. Around 140–150 ms, both wavelengths show an abrupt transverse redistribution, consistent with the emittance exchange process.

The experimental results are compared with simulations including the effects of adiabatic damping and synchrotron-radiation damping. Since emittance exchange is not included in the simulations, the comparison is restricted to camera delays below 140 ms. The comparison is shown in Fig. 3. The vertical plane shows better agreement with the model: although the measured size is 25% to 30% smaller than expected at the beginning of the ramp, it fol-

lows the predicted damping trend within about ≤10% between 50 ms and 90 ms. In contrast, the horizontal size remains larger than predicted near the end of the pre-exchange region. Around 110 ms to 120 ms, the model predicts $\sigma_x \simeq 160\,\mu\text{m}$ to 170 µm, while the measured values remain near (287.4 ± 0.9)–$(324.4 \pm 0.3)\,\mu\text{m}$. Some discrepancy is expected, since the simulations assume equal horizontal and vertical emittances at injection, whereas LINAC measurements indicate that the horizontal emittance is typically larger than the vertical one. However, the observed difference is larger than anticipated. This is particularly relevant because the emittance ε_x is inferred from σ_x^2 after subtracting the dispersive contribution; therefore, a sizeable disagreement in the measured beam size can translate into a significantly larger deviation in the calculated emittance. The present measurements would indicate a horizontal emittance about a factor of 4 to 5 larger than expected, motivating further investigation.

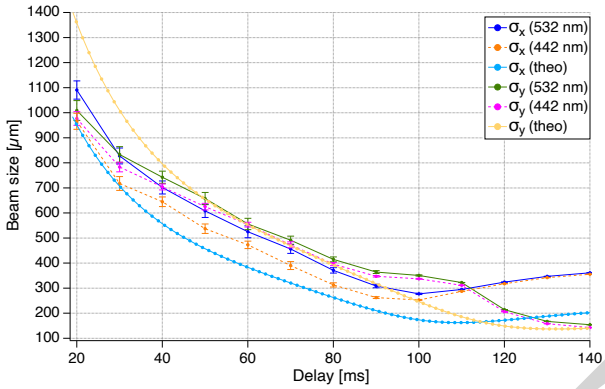

Figure 3: Measured and theoretical beam size evolution during the ramp up to 140 ms.

In contrast, resolving the emittance exchange dynamics during coupling resonance crossing required short exposures of 27 µs and 50 µs, corresponding to integration over only a few tens of turns. As shown in Fig. 4, the beam sizes remain nearly constant before the exchange process begins. For the 50 µs exposure, between 140 and 146 ms the horizontal and vertical beam sizes are approximately $\sigma_x = (360.3 \pm 0.5)\,\mu\text{m}$ and $\sigma_y = (147.7 \pm 0.3)\,\mu\text{m}$. After about 146 ms, the exchange process becomes visible: σ_x decreases while σ_y increases rapidly. The minimum horizontal beam size is reached at approximately 148.8 ms, where $\sigma_x = (287.4 \pm 0.7)\,\mu\text{m}$, corresponding to a reduction of about 20% relative to the pre-exchange value. Although this reduction in beam size is modest, it corresponds to a much larger decrease in the inferred horizontal emittance because the horizontal beam size includes a significant dispersive contribution at this location. At the same time, the vertical beam size reaches $\sigma_y = (422.1 \pm 0.5)\,\mu\text{m}$, an increase of about 186%. The 27 µs exposure shows the same behavior, with a minimum horizontal size of $\sigma_x = (294.1 \pm 1.2)\,\mu\text{m}$ and a maximum vertical size of $\sigma_y = (431.8 \pm 1.4)\,\mu\text{m}$ at 148.8 ms. These measurements confirm that the monitor resolves the fast transverse redistribution associated with emittance exchange, and that the optimum extraction timing corresponds to the minimum horizontal beam size, around 148.7 ms.

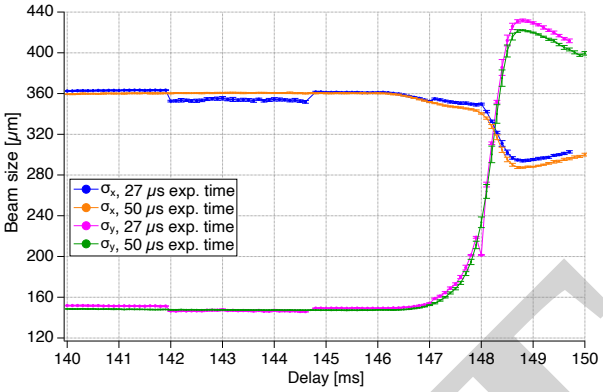

Figure 4: Emittance exchange dynamics at 27 µs and 50 µs exposure times with a 532 nm bandpass filter.

CONCLUSION

The visible light monitor developed for the SLS booster successfully resolves the transverse beam profile throughout the acceleration ramp and during the fast emittance exchange process. Measurements at 442 nm and 532 nm demonstrate that the present extraction timing, around 148.7 ms, coincides with the minimum horizontal beam size, with σ_x reduced by about 20% relative to the pre exchange value. This directly supports the use of the monitor for optimizing booster extraction and injection into the storage ring.

Comparison with simulations shows a better agreement in the vertical plane than in the horizontal one, although the smaller measured vertical size at early times remains unexplained. The horizontal discrepancy is especially relevant for emittance determination. The present correction includes depth of field and curvature contributions only; future work will quantify spherical aberration from the large aperture plano convex lens to improve absolute emittance estimates.

ACKNOWLEDGEMENTS

The authors would like to thank Cigdem Ozkan Loch for her key contributions to the design and implementation of the system. We are also grateful to Friederike Ewald at the ESRF for sharing her experience with SR diagnostics in the ESRF booster ring, which provided valuable guidance for the design of our system.

REFERENCES

[1] W. Joho, M. Muñoz, and A. Streun, "The SLS Booster Synchrotron", *Nucl. Instrum. Methods Phys. Res. A*, vol. 562, no. 1, pp. 1–11, 2006. doi:10.1016/j.nima.2006.01.129

[2] J. Kallestrup and M. Aiba, "Emittance exchange in electron booster synchrotron by coupling resonance crossing", *Phys. Rev. Accel. Beams*, vol. 23, no. 2, p. 020701, 2020. doi:10.1103/PhysRevAccelBeams.23.020701

[3] J. Kallestrup, "Emittance exchange through coupling resonance crossing in electron synchrotrons", Ph.D. thesis, ETH Zürich, 2021. doi:10.3929/ethz-b-000532923

[4] B. K. Scheidt, "Dipole light monitor system for the ESRF injector", in *Proc. DIPAC'05*, Lyon, France, pp. 24–26, Jun. 2005.

[5] J. g, W. Berg, J. R. Calvey, K. C. Harkay, and K. P. Wootton, "Measurements of bunch length in the Advanced Photon Source Booster Synchrotron", in *Proc. NAPAC'22*, Albuquerque, NM, USA, pp. 394–397, Aug. 2022. doi:10.18429/JACoW-NAPAC2022-TUPA22

[6] A. Moutardier *et al.*, "Study of Visible Synchrotron Radiation Monitor on SOLEIL Booster", in *Proc. IBIC'23*, Saskatoon, Canada, pp. 331–334, Sep. 2023. doi:10.18429/JACoW-IBIC2023-WEP002

[7] T. Schiffer, W. Hillert, P. Hänisch, and M. T. Switka, "Set up of a synchrotron light monitor at the 2.5 GeV booster synchrotron at ELSA", in *Proc. IPAC'14*, Dresden, Germany, pp. 3468–3470, Jun. 2014. doi:10.18429/JACoW-IPAC2014-THPME098

[8] J. A. Clarke, "A review of optical diagnostics techniques for beam profile measurements", in *Proc. EPAC'94*, London, UK, p. 1643, Jun. 1994.

[9] A. Hofmann and F. Méot, "Optical resolution of beam cross-section measurements by means of synchrotron radiation", *Nucl. Instrum. Methods Phys. Res.*, vol. 203, no. 1, pp. 483–493, 1982. doi:10.1016/0167-5087(82)90663-9